Proceedings of ASME Turbo Expo 2011
GT2011
June 6-10, 2011, Vancouver, British Columbia, Canada

GT2011-46297

NATURAL FREQUENCY SHIFT IN A CENTRIFUGAL COMPRESSOR IMPELLER FOR HIGH-DENSITY GAS APPLICATIONS

Yohei Magara
Kazuyuki Yamaguchi
Hitachi, Ltd.
Mechanical Engineering Research Laboratory
832-2 Horiguchi, Hitachinaka, Ibaraki 312-0034, Japan
yohei.magara.bc@hitachi.com

Haruo Miura
Naohiko Takahashi
Mitsuhiro Narita
Hitachi Plant Technologies, Ltd.
603 Kandatsu-machi, Tsuchiura-shi, Ibaraki 300-0013, Japan

ABSTRACT

In designing an impeller for centrifugal compressors, it is important to predict the natural frequencies accurately in order to avoid resonance caused by pressure fluctuations due to rotor-stator interaction. However, the natural frequencies of an impeller change under high-density fluid conditions. The natural frequencies of pump impellers are lower in water than in air because of the added mass effect of water, and in high-pressure compressors the mass density of the discharge gas can be about one-third that of water. So to predict the natural frequencies of centrifugal compressor impellers, the influence of the gas must be considered. We previously found in the non-rotating case that some natural frequencies of an impeller decreased under high-density gas conditions but others increased and that the increase of natural frequencies is caused by fluid-structure interaction, not only the added mass effect but also effect of the stiffness of the gas. In order to develop a method for predicting natural frequencies of centrifugal compressor impellers for high-density gas applications, this paper presents experimental results obtained using a variable-speed centrifugal compressor with vaned diffusers. The maximum mass density of its discharge gas is approximately 300 kg/m^3. The vibration stress on an impeller when the compressor was speeding up or slowing down was measured by strain gages, and the natural frequencies were determined by resonance frequencies. The results indicate that for high-density centrifugal compressors, some natural frequencies of an impeller increased in high-density gas. To predict this behavior, we developed a calculation method based on the theoretical analysis of a rotating disc. Its predictions are in good agreement with experimental results.

NOMENCLATURE

A_d	: disc surface area
A_R	: rigid surface of cylindrical enclosure
c	: sound velocity
h_s	: disc thickness
h_f	: gap length
L, M	: coupling factor
m	: number of nodal circles
n	: number of nodal diameters
$\mathbf{n}$	: unit normal vector for the boundary surface
t	: time
V	: volume of enclosure
w	: transverse displacement of disc
ρ_s	: disc density
ρ_f	: gas density
ϕ	: velocity potential
ω	: angular frequency
ω^s	: uncoupled natural frequency of disc
ω^f	: uncoupled acoustic resonance frequency of gas
Φ	: uncoupled natural mode of gas
Ψ	: uncoupled natural mode of disc
$(\dot{\ })$	: temporal derivatives

INTRODUCTION

The centrifugal compressors for gas injection aimed at enhanced oil recovery, gas lift, and underground storage of carbon dioxide gas are required for extremely high-pressure operation. For such compressors, the mass density of their discharge gas can be about 300 kg/m^3, which is nearly one-third that of water. The natural frequencies of impellers operating under such high-density fluid conditions are shifted by the influence of the fluid. For instance, it is known that the natural frequencies of pump impellers are lower in water than in air because of the added-mass effect of water [1] [2]. There is also a report that the natural frequencies of centrifugal compressor impellers decreased with increasing gas pressure and gas density [3]. A study of a structure-acoustic coupling system (i.e., a structure-gas coupling system) indicated that the natural frequencies of some coupled vibration modes are higher than those of uncoupled modes [4].

In designing an impeller for centrifugal compressors, the natural frequencies under high-gas-density conditions should be predicted accurately so that resonance caused by the fluid exciting force due to rotor-stator interaction can be avoided. To develop a method for predicting natural frequencies of centrifugal compressor impellers for high-density gas applications, in previous research we experimentally investigated the characteristics of the natural frequencies of a low-specific-speed two-dimensional closed impeller and an equivalent disc in the non-rotating case and found that in high-density gas some natural frequencies of the impeller and the disc decreased but others increased [5]. We also observed some resonance frequencies, under high-gas-density conditions that we did not observe under low-gas-density conditions. These behaviors of natural frequencies can be explained by considering the coupling vibration between the impeller vibrational displacement and the pressure fluctuations of the surrounding gas. That is, the impeller vibration couples with acoustic resonance occurring in the space between the impeller and the casing wall.

In this paper we describe the experimental results obtained when we investigated natural frequency shifts of an impeller in the rotating case by using a test centrifugal compressor with vaned diffusers. The results indicate that for high-density centrifugal compressors, some natural frequencies of an impeller increase in high-density gas. To predict this behavior, we developed a calculation method based on the theoretical analysis of a rotating disc. Its predictions are in good agreement with experimental results.

EXPERIMENTAL APPARATUS AND PROCEDURES

To investigate the behavior of natural frequencies of a centrifugal compressor impeller, a test compressor has been developed. The test compressor is a single-shaft three-stage centrifugal compressor driven by an electric motor. A picture of the test compressor is shown in Figure 1. The compressor has a barrel casing using a shear key structure, and the outer diameter of the casing is about 1.5 meter. Figure 2 shows the three-dimensional model of the test compressor. The impellers are typical low-specific-speed two-dimensional closed impellers having eleven blades. In each stage there is a diffuser with nineteen vanes downstream of the impeller, and there are return vanes upstream of the second and third stage impeller inlets. The specifications of the compressor are listed in Table 1. The rotation speed is controlled by an inverter-driven motor. The compressor operated in closed loop. The pressure and mass density of the discharge gas are changed by adjusting the suction pressure and temperature and can be as high as 20 MPa and 287 kg/m^3, respectively.

Figure 1 Test compressor.

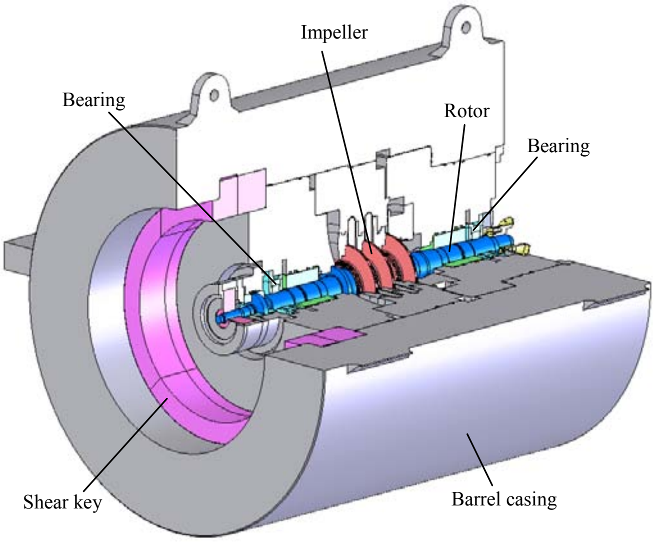

Figure 2 Three-dimensional model of test compressor.

Table 1 Specification of test compressor.

Motor power	1,760 kW
Impeller outer diameter	310 mm
Number of stages	3
Number of impeller blades	11
Number of return vanes	14
Number of diffuser vanes	19
Maximum continuous speed	14,805 min^{-1}
Working gas	Carbon dioxide (CO_2)
Suction / Discharge pressure	Approx. 6 / 20 MPa
Max. design mass density of gas	287 kg/m^3

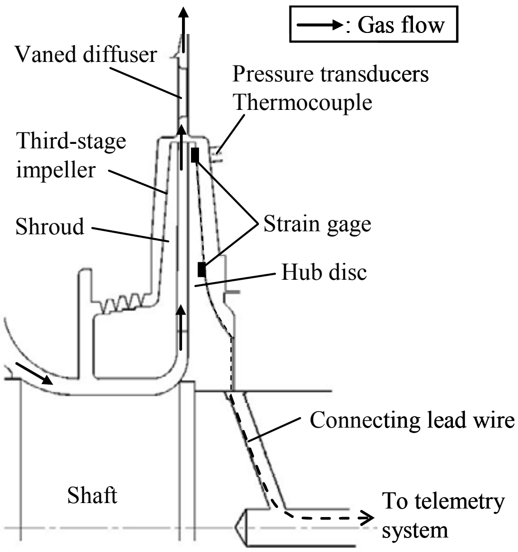

Figure 3 Flow path in the third stage.

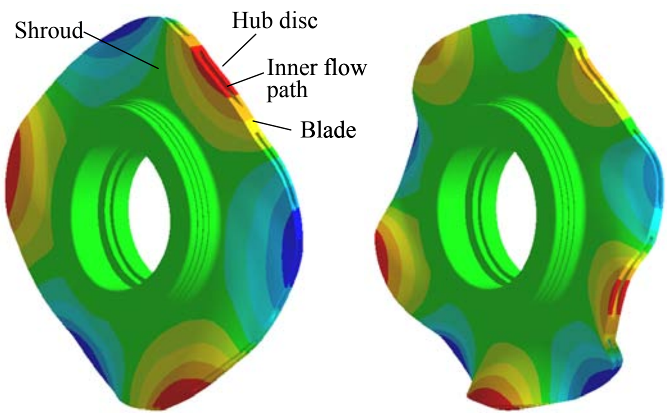

Figure 4 Vibrational mode shapes of impeller with 3 (left) and 5 (right) nodal diameters.

The vibration measurements were carried out at the third stage because that is where the gas density is highest and thus where the influence of the gas on the natural frequencies is largest. Figure 3 shows the flow path in the third stage. The flow from the second stage is guided to the impeller inlet, compressed and accelerated by the rotating impeller, and discharged into the diffuser. Here the impeller is excited by the fluid exciting force (i.e., pressure fluctuation) caused by the interaction between the impeller blades and the diffuser vanes.

The excited vibration modes of the impeller have zero or more nodal diameters and the number of nodal diameters n depends on the relation between the number of the impeller blades and the diffuser vanes. This is expressed by the equation below [6]:

$$h_1 Z_s \pm n = h_2 Z_r \tag{1}$$

where Z_s and Z_r are respectively the numbers of diffuser vanes and impeller blades and where h_1 and h_2 are integers indicating particular harmonic orders of the blade- and vane-passing frequency. The sign of n depends on the traveling direction of the wave excited on the impeller disc: plus indicates that the wave travels in the same direction as the rotation of the rotor (i.e., that the wave is a forward-traveling wave), and minus indicates that the wave travels in the direction opposite the rotation of the rotor (i.e., that the wave is a backward-traveling wave).

In our experiment the number of the impeller blades Z_r is 11 and the number of the diffuser vanes Z_s is 19. From the equation (1), the resonances of the three-diameter mode and five-diameter mode are caused in the operating range of the test compressor. The vibration modes with nodal diameters computed by FEM code, ANSYS® Multiphysics™ [7], are shown in Figure 4. The contour plots show the amplitude of the axial displacement. The natural frequencies of the impeller that were measured in a hammering test under atmospheric conditions are listed in Table 2.

Figure 5 is an example of a relation between the rotation speed and the 19th- and 38th-order vibrational stresses obtained experimentally. Because that the impeller is excited by pressure fluctuation when the impeller blades pass by the diffuser vanes,

Table 2 Measured natural frequencies of the impeller under atmospheric conditions

Nodal diameter	Natural frequency [Hz]
1	1414
2	2233
3	3501
4	4419
5	5328

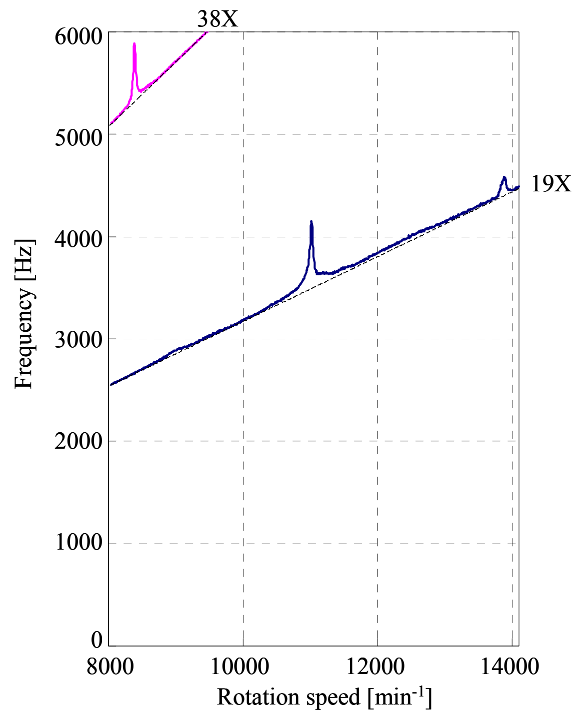

Figure 5 Relation between the rotation speed and the 19th- and 38th-order vibrational stresses (Suction pressure: 0.2 MPa).

the 19th harmonic of the rotation speed is a fundamental frequency.

The natural frequencies of the impeller of the test compressor in operation were obtained by the speed at which resonance occurred. Under the high-density conditions, the vibration response of the five-nodal-diameter mode was small because the fluid exciting force was relatively weak due to the lower resonant speed. Therefore in this paper the results of the three-nodal-diameter mode of the impeller are presented.

The strain gages installed on the impeller as shown in Figure 3 were used to measure the vibration stress when the compressor was speeding up or slowing down. The acceleration rate was set to a constant value, approximately 4.4 min^{-1} per second. A picture of the test rotor is shown in Figure 6. The strain gages and the connecting lead wires were protected by stainless steel foil, and the signals from the strain gages were transmitted by wires through the center hole of the shaft to the telemetry system mounted at the end of the rotor. Figure 7 shows the locations of the strain gages. We used four strain gages (numbered from SG-01 to SG-04) to identify the vibrational modes of the impeller. SG-01 and SG-02 measured the circumferential stress, and SG-03 and SG-04 measured the radial stress. Here, in order to identify the vibration mode which is excited in operation, we consider the case in which the impeller hub disc vibrates with a natural frequency ω_n, having n nodal diameters. In a rotating coordinate system the circumferential mode of vibration, y, is represented by:

$$y = \cos(n\theta \pm \omega_n t) \tag{2}$$

where θ indicates the circumferential location along with the rotating direction and t is time. The plus/minus sign indicates the traveling direction of the vibration wave, plus meaning that the wave is a backward-traveling wave (traveling in the $-\theta$ direction) and minus meaning that the wave is a forward-traveling wave (traveling in the $+\theta$ direction). Here the time waveforms observed at the points of $\theta = \theta_0$ and θ_1 follow the expressions:

$$y = \cos(\omega_n t \pm n\theta_0) \ \text{ at } \theta = \theta_0 \tag{3}$$

and

$$y = \cos(\omega_n t \pm n\theta_0 \pm n\Delta\theta) \ \text{ at } \theta = \theta_1 \tag{4}$$

where $\Delta\theta$ is the angular difference between the two observation points (θ_1 - θ_0). The phase difference φ between the two points is expressed as:

$$\varphi = \pm n\Delta\theta + 2k\pi , \tag{5}$$

and k ranges over all integers. In addition, in the test compressor, there are two measuring directions for the strain gages: circumferential and radial. The phases differ from each other by 180 degrees because the stresses of compression and tension are opposite. As a result, the relative phase differences of the disc vibration are obtained for each mode. The phase differences with respect to the location of 72 deg (that of SG-02) are listed in Table 3.

The gas pressure and temperature around the impeller were measured using a static pressure transducer and a thermocouple installed in the wall of the hub-disc side. The gas density and the sound velocity were calculated from the pressure and temperature using W-PROPATH [8]. The pressure fluctuation in the space between the impeller hub disc and the casing wall was also measured and investigated.

Figure 6 Rotor of the test compressor

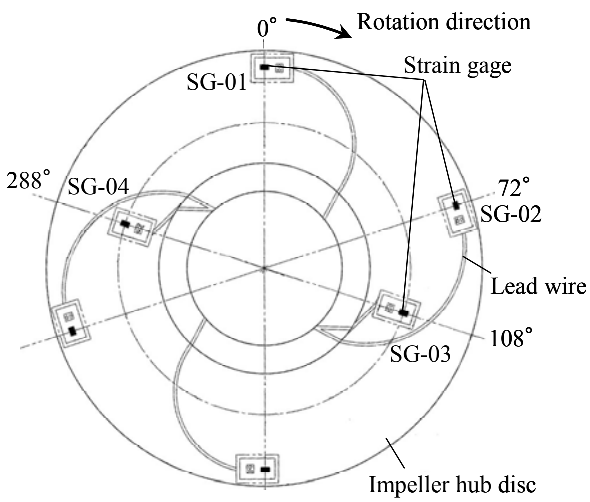

Figure 7 Strain gage measuring points.

Table 3 Phase difference of the hub disc vibration relative to that at 72 deg.

Corresponding gage	SG-01	SG-02	SG-03	SG-04
Location [deg]	0	72	108	288
Direction	Circumferential		Radial	
3 nodal diameters	−144	0	72	−108
5 nodal diameters	0	0	0	180

EXPERIMENTAL RESULTS

The natural frequency shift of the impeller in operation was investigated by order tracking analysis, the results of which are shown in Figure 8 and Figure 9. Figure 8 shows how the 19th-order amplitude of vibrational stresses measured by SG-04 changes with rotation speed under the different pressure conditions. As shown in Figure 8(a), under low-pressure conditions the resonance occurs at 11050 min^{-1}. From this, the natural frequency of the 3-nodal-diameter mode of the impeller is determined to be 3499 Hz, about the same as that under atmospheric conditions (3501 Hz). It is understood that the centrifugal force hardly influences the natural frequency of the impeller. In addition, in this case the mass density of the surrounding gas of impeller was 9 kg/m^3. This is much lower than that of the stainless steel impeller, and the gas has little influence on the natural frequency. The results obtained at higher suction pressures are shown from Figure 8(b) to 8(d). As the pressure increases, the peak becomes less sharp but higher. The reason for this is thought to be since the gas density increases, the fluid damping gets larger while the fluid exciting force also increases. Moreover, the peak of the amplitude shifts to higher speeds. That is, the resonance frequency increases. In the case of a 6 MPa suction pressure, the gas density became 202 kg/m^3. If the natural frequency shifts of the impeller depend on only the added mass effect, the resonance frequency must decrease as the gas density increases. However, the resonance frequency is 3741 Hz at 11813 min^{-1} which indicates a 6.9 % increase compared with the natural frequency of the impeller with three nodal diameters in air. This cannot be explained by only the added mass effect.

Figure 9 shows the relative phase differences of 19th-order impeller vibration with respect to SG-02. Except at the 0.2 MPa suction pressure, SG-01 did not work well, so the results obtained with SG-01 are excluded from the graphs. The rotation speed which the resonance occurred is indicated by a vertical line in each plot. One sees in Figure 9(a) that the relative phase differences are held in stable positions at the resonance speed. The phase differences at the resonance are summarized in Table 4. These differences are approximately the same regardless of the pressure conditions and are nearly equal to those of the

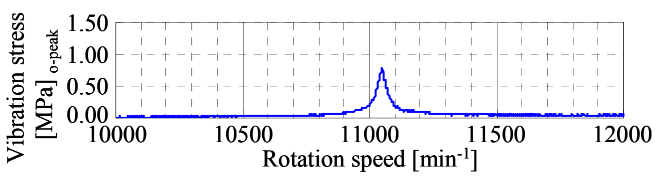

(a) Suction pressure: 0.2 MPa (Discharge pressure: 0.6 MPa)

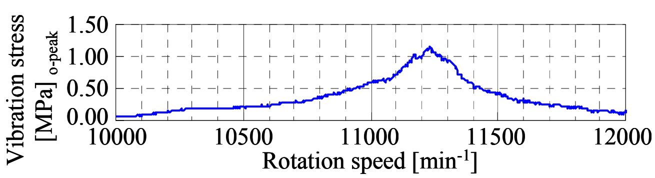

(b) Suction pressure: 2 MPa (Discharge pressure: 3.5 MPa)

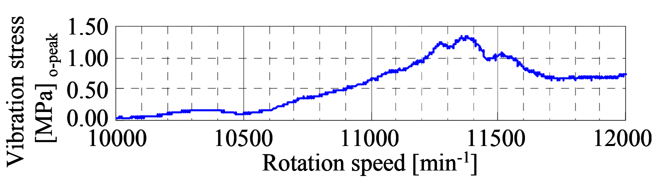

(c) Suction pressure: 4 MPa (Discharge pressure: 7.0 MPa)

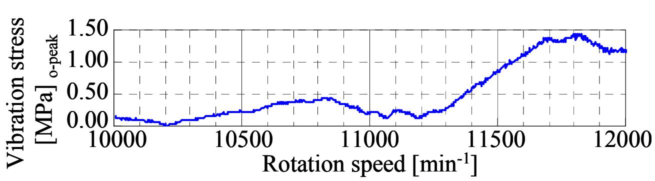

(d) Suction pressure: 6 MPa (Discharge pressure: 11.3 MPa)

Figure 8 19th-order (i.e., diffuser vane passing frequency) amplitude of impeller vibration during acceleration.

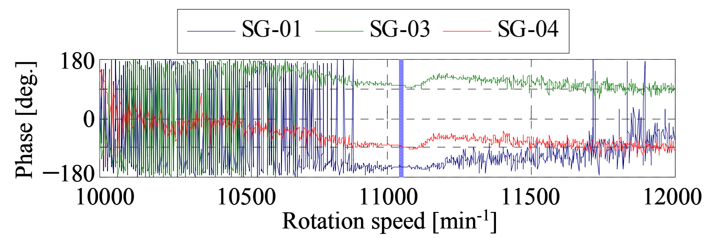

(a) Suction pressure: 0.2 MPa (Discharge pressure: 0.6 MPa)

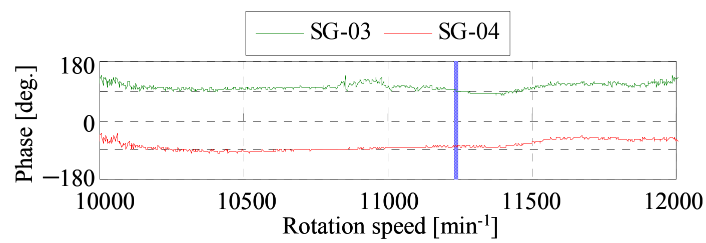

(b) Suction pressure: 2 MPa (Discharge pressure: 3.5 MPa)

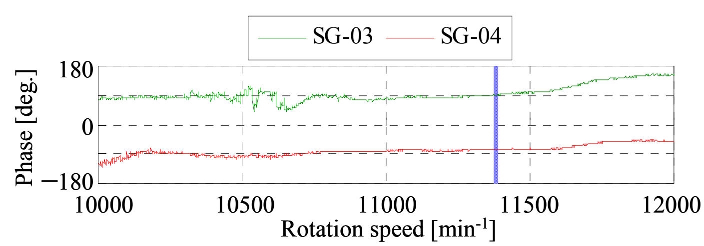

(c) Suction pressure: 4 MPa (Discharge pressure: 7.0 MPa)

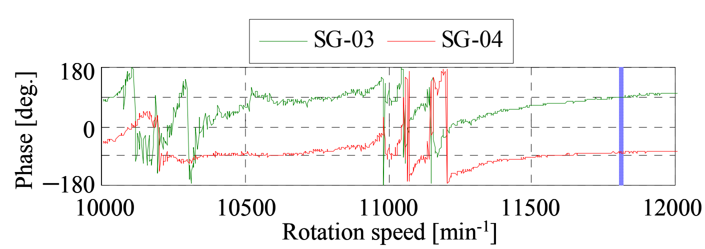

(d) Suction pressure: 6 MPa (Discharge pressure: 11.3 MPa)

Figure 9 Phase difference of 19th-order impeller vibration relative to that at SG-02.

Table 4 Phase difference at the resonance frequency relative to that at SG-02.

Suction Pressure [MPa]	Relative phase difference [deg]			
	SG-01	Sg-02	SG-03	SG-04
0.2	−148	0	101	−86
2	---	0	88	−80
4	---	0	91	−77
6	---	0	93	−79

vibration mode of a disc with three-nodal diameters as described earlier (see Table 3). The disagreement between the calculated and the experimental values is considered to be caused by the difference between a disc and the impeller; that is, the stiffness of the impeller hub disc is not uniform circumferentially because of the effect of the blades. From these results the peaks seen in Figure 8 are identified as being due to the mode with three nodal diameters. Therefore, it is concluded that the natural frequency of the 3-nodal-diameter mode of the impeller increases.

FLUID-STRUCTURE INTERACTION ANALYSIS

Although the added-mass effect of fluid does not cause an increase in the natural frequencies, the natural frequency of the impeller with three nodal diameters in high-pressure gas increased. We therefore thought that the compressibility of the gas has an additional effect on the frequencies. In our previous study we applied the theoretical approach used to determine the vibrations of a disc in a gas-filled enclosure [9] to the problem of the natural-frequency shift of a non-rotating disc, and we were able to explain the mechanism of the natural frequencies shift by considering the coupling between the gas and disc [5]. In this paper we present a method for predicting the natural frequencies of the impeller in operation (i.e., rotating).

Analytical model

For simplicity, we consider the impeller a disc as shown in Figure 10. The disc is rotating at a constant angular velocity Ω_s and the surrounding gas is assumed to be swirling as a bulk flow at an angular velocity Ω_f. The cylindrical coordinate system (r, θ, z) is used. The space surrounded by the wall of the cylindrical enclosure and the disc corresponds to the side gap between the impeller and the casing wall. This space is assumed to be symmetrical with respect to the disc, and the gas is assumed to be inviscid and compressible.

Governing equation for surrounding gas

In the coordinate system (r, η, z) that rotates with the gas swirl (we call it the gas coordinate system), the coupled wave equation and boundary conditions for the gas in the left gap are given by:

$$\nabla^2\phi = \frac{1}{c^2}\ddot{\phi} \quad \text{with} \quad \nabla\phi\cdot\mathbf{n} = \begin{cases} 0 & \text{on } A_R \\ \dot{w} & \text{on } A_s \end{cases}. \tag{6}$$

The coupled velocity potential of the gas, ϕ, and transverse displacement of the disc, w, are expressed by using superposition of the uncoupled natural modes:

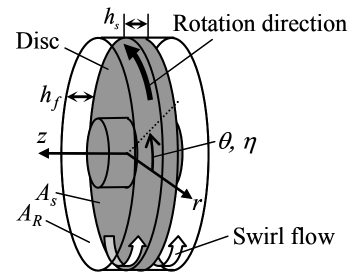

Figure 10 Schematic diagram of a disc in a gas-filled cylindrical enclosure.

$$\begin{cases} w = \sum_m \sum_n \{C_{mn}(t)\cos n\eta + S_{mn}(t)\sin n\eta\} R^s_{mn}(r) \\ \phi = \sum_m \sum_n \{\alpha_{mn}(t)\cos n\eta + \beta_{mn}(t)\sin n\eta\} R^f_{mn}(r) \end{cases} \tag{7}$$

where C_{mn}, S_{mn}, a_{mn}, and b_{mn} are the superposition coefficients, which are functions of time. The indexes m and n are respectively the number of nodal circles and the number of nodal diameters. R_{mn} indicates the uncoupled vibration mode in the radial direction. The superscripts s and f respectively indicate the structure and fluid modes (i.e., the disc and gas).

Now we apply Green's theorem to expression (8), where Φ_{ql} is the uncoupled natural mode of the gas. q is the number of nodal circles and l is the number of nodal diameters. Then we obtain equation (9). Equation (10) is derived by substituting the coupled and uncoupled wave equations and the boundary conditions into equation (9).

$$\Phi_{ql}\nabla^2\phi - \phi\nabla^2\Phi_{ql} \tag{8}$$

$$\int_V (\Phi_{ql}\nabla^2\phi - \phi\nabla^2\Phi_{ql})dV = \int_{A_s+A_R} (\Phi_{ql}\nabla\phi\cdot\mathbf{n} - \phi\nabla\Phi_{ql}\cdot\mathbf{n})dA \tag{9}$$

$$\frac{1}{c^2}\int_V \{\Phi_{ql}\ddot{\phi} + (\omega^f_{ql})^2\phi\Phi_{ql}\}dV = \int_{A_s} \Phi_{ql}\dot{w}dA \tag{10}$$

The uncoupled natural mode of the gas is written as follows:

$$\Phi_{ql} = R^f_{ql}(r)\cdot\cos l\eta \;,\; R^f_{ql}(r)\cdot\sin l\eta \tag{11}$$

Substituting equations (7) and (11) into equation (10), we obtain

$$\ddot{\alpha}_{ql} + (\omega^f_{ql})^2\alpha_{ql} = \frac{c^2}{h_f}\sum_m \frac{L_{qml}}{M^f_{ql}}\dot{C}_{ml} \;, \tag{12}$$

$$\ddot{\beta}_{ql} + (\omega^f_{ql})^2\beta_{ql} = \frac{c^2}{h_f}\sum_m \frac{L_{qml}}{M^f_{ql}}\dot{S}_{ml} \;. \tag{13}$$

Here L and M^f are the coefficients expressing the intensity of coupling between the disc and gas, defined as

$$L_{qml} = \int \{R^f_{ql}(r)\cdot R^s_{ml}(r)\} r dr \tag{14}$$

and

$$M^{f}_{ql} = \int \{R^{f}_{ql}(r)\}^2 r dr \,. \tag{15}$$

Equation of motion for a rotating disc

Now we consider the gas-disc interaction and assume that the pressure distributions in the left and right regions fluctuate out-of-phase with each other. In the gas coordinate system, we obtain the following equation of motion for the lateral vibration of a disc:

$$\rho_s h_s (\ddot{w} + 2\Omega_0 \frac{\partial \dot{w}}{\partial \eta} + \Omega_0^2 \frac{\partial^2 w}{\partial \eta^2}) + D\nabla^4 w = -2\rho_f \dot{\phi} \,, \tag{16}$$

where D is the bending stiffness of the disc, ρ_s and ρ_f are respectively the densities of the disc and of the gas, and Ω_0 is the difference between the angular velocities of the rotating disc and the swirl of gas:

$$\Omega_0 = \Omega_s - \Omega_f \,. \tag{17}$$

Substituting equation (7) into equation (16), multiplying equation (16) by the right side of equation (18), and then integrating both sides, we can obtain equations (19) and (20).

$$\Psi_{ql} = R^{s}_{ql}(r) \cdot \cos l\eta \;,\; R^{s}_{ql}(r) \cdot \sin l\eta \tag{18}$$

$$\ddot{C}_{ql} + 2l\Omega_0 \dot{S}_{ql} + \{(\omega^{s}_{ql})^2 - (l\Omega_0)^2\} C_{ql} = -2 \frac{\rho_f}{\rho_s h_s} \sum_m \frac{L_{mql}}{M^{s}_{ql}} \dot{\alpha}_{ml} \tag{19}$$

$$\ddot{S}_{ql} + 2l\Omega_0 \dot{C}_{ql} + \{(\omega^{s}_{ql})^2 - (l\Omega_0)^2\} S_{ql} = -2 \frac{\rho_f}{\rho_s h_s} \sum_m \frac{L_{mql}}{M^{s}_{ql}} \dot{\beta}_{ml} \tag{20}$$

where M^s is defined as below:

$$M^{s}_{ql} = \int \{R^{s}_{ql}(r)\}^2 r dr \,. \tag{21}$$

Uncoupled natural frequency of the impeller and the gas

The natural frequencies of the coupled system are obtained by solving simultaneous equations (12), (13), (19), and (20). Until this point, we have considered the case of a disc and developed the expressions for the coupled system between the disc and gas. With a little ingenuity, however, one can apply these expressions to the coupled system between the impeller and its surrounding gas.

First we use the uncoupled natural frequencies of the impeller and the acoustic resonance frequencies of the impeller side gap as ω^s and ω^f in the previous equations. Then we calculate the coupling coefficients L and M from the actual mode shapes of the impeller vibration and the acoustic mode shapes in the side gap.

The frequencies listed in Table 2 are regarded as the uncoupled frequency of the impeller because the gas density is negligibly low under atmospheric conditions. Here we don't take into account the vibration modes of the impeller with one or more nodal circles because their natural frequencies are relatively much higher. The uncoupled acoustic resonance frequencies and the uncoupled mode shapes are obtained by a finite element analysis. The uncoupled resonance frequencies of the acoustic mode with three nodal diameters are listed in Table 4. Figure 11 shows the acoustic mode shapes with three nodal diameters and zero nodal circles in the impeller side gap calculated by acoustic analysis of ANSYS® Multiphysics™ [7]. The contour plots show the amplitude of pressure fluctuations on the surface of the impeller. The cross-sectional view of the analytical model, presenting the relationship between the instantaneous pressure distributions of the shroud side and of the hub side, is shown in Figure 12. Because of the pressure differential between the shroud side and the hub side, the fluid force acts on the impeller, and therefore the natural frequencies of the impeller are affected by the surrounding gas.

Table 5 Acoustic resonance frequencies of the 3-nodal-diameter mode in the impeller side gap with a sound velocity of 316 m/s.

Nodal circles	Resonance frequency [Hz]
0	1721
1	3306
2	5167
3	7072
4	9007

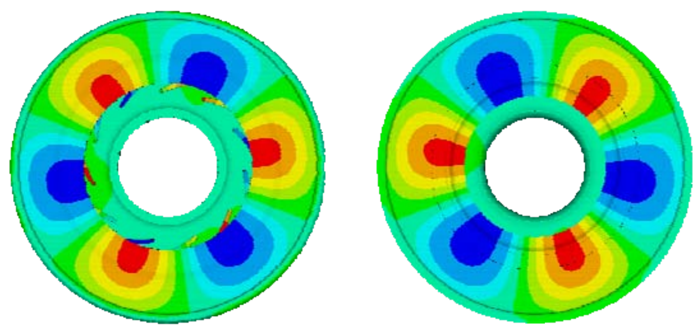

Figure 11 Acoustic mode shapes with three nodal diameters and zero nodal circles in the impeller side gap (Left: shroud side, Right: hub-disc side).

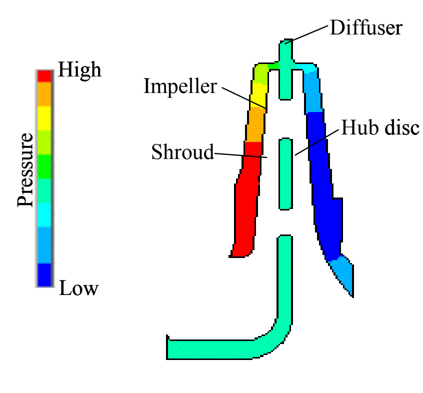

Figure 12 Instantaneous distribution of fluctuating pressure.

Figure 13 shows how the coupling factor L varies with the number of the nodal circles of the acoustic resonance mode. From the graph one sees that when the number of the nodal circles is one the intensity of coupling is highest and that the influence of the modes with two or more nodal circles is small. In addition, we know from solving the equations that the intensity of coupling becomes stronger as the uncoupled natural frequencies of the impeller and of the acoustic become closer each other. Just be forewarned that the acoustic resonance frequencies are proportional to the sound velocity.

The relation between the number of the modes used for calculation and the calculated results for the vibration mode of the impeller with three nodal diameters is shown in Figure 14, where the vertical axis indicates the dimensionless natural frequency normalized by the natural frequency obtained under atmospheric conditions. One sees there that the calculated natural frequency becomes almost constant above three modes used. That is, we consider only the acoustic modes having from zero to two nodal circles. This is because the natural frequency of the three-nodal-diameter mode of the impeller lies between that of the one-nodal-circle mode of the acoustic and that of the two-nodal-circle mode.

EXPERIMENTAL RESULTS AND CALCULATIONS

A comparison between the experimental results and the calculation results of the natural frequencies of the impeller with three nodal diameters is shown in Figure 15. The vertical axis is the dimensionless natural frequency obtained in the same way as that in Figure 14. The plots of the experimental results were obtained by identifying the peak frequencies from the tracking analysis. Also shown there are the results obtained by changing the suction temperature. It is clear that the natural frequency of the impeller increases as the mass density of the gas increases. The maximum rate of the natural frequency shift is 6.9 % at ρ_f=202 kg/m^3, c=278 m/s.

The calculation results are also shown in Figure 15. At each point the measured density and sound velocity were used for calculations. In the calculation results as well as with the experimental results, the higher the gas density becomes, the higher the natural frequency is. The calculation tends to overestimate the coupled natural frequency. This is thought to be due to supposing ideal conditions when calculating the intensity of coupling. Because the swirl flow is actually turbulent to some extent, the intensity of coupling becomes weaker. One sees in figure 15 that the natural frequencies can be predicted with errors less than 4 %.

CONCLUSION

To develop a method for predicting the natural frequencies of centrifugal compressor impellers for high-density gas applications, we investigated the characteristics of the natural frequencies of an impeller in operation by using a single-shaft three-stage centrifugal compressor. Measuring the natural frequencies of the impeller in operation under high-density conditions, we found that the natural frequency of the 3-nodal-diameter mode of the impeller increased as the gas density

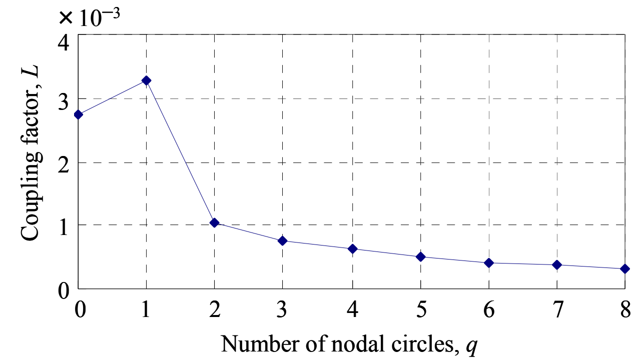

Figure 13 Coupling factor L between the gas and the impeller vibration for the mode with three nodal diameters.

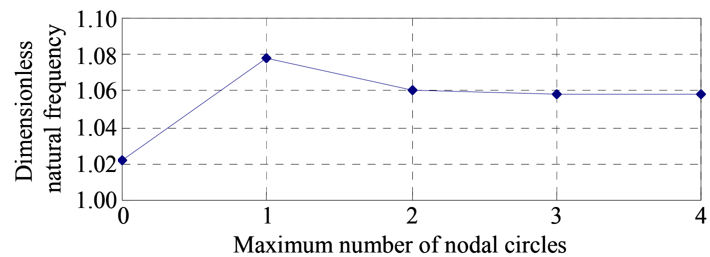

Figure 14 Relation between the number of the modes used for calculation and the calculated results for the mode with three nodal diameters (ρ_f=179 kg/m^3, c=277 m/s).

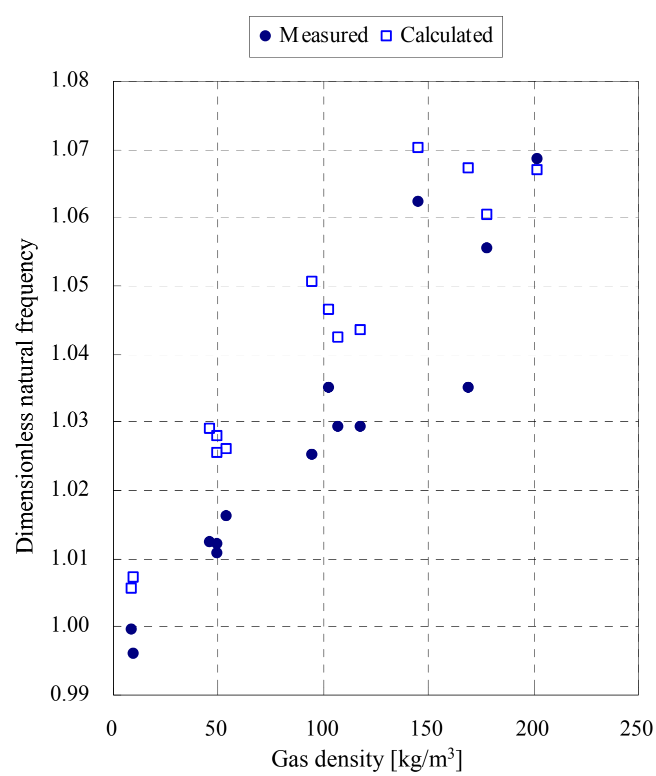

Figure 15 Comparison of experimental and calculation results of the natural frequencies of the impeller with three nodal diameters.

increased. These results are consistent with our previous experimental results obtained in the non-spinning case.

To predict the natural frequency shift, a fluid-structure interaction analysis method was developed by considering the coupling between the impeller and the surrounding gas. The calculation results obtained using the method agreed well with the experimental results.

ACKNOWLEDGMENTS

We thank Professor Shigehiko Kaneko of the University of Tokyo, Professor emeritus Hiroshi Kanki of Kobe University, and Professor emeritus Osami Matsushita of the National Defense Academy of Japan for their helpful advice.

REFERENCES

[1] Guo, S. and Maruta, Y., 2005, "Experimental Investigations on Pressure Fluctuations and Vibration of the Impeller in a Centrifugal Pump with Vaned Diffusers", *JSME International Journal Series B*, Vol. 48, Issue 1, pp. 136-143.

[2] Inagaki, T., Oda, T., and Kawakami, T., 1989, "Additional Water Mass in Pump Impeller Vibration", *Transactions of the Japan Society of Mechanical Engineers Series C*, Vol. 55, No. 511, pp. 651-655.

[3] Kawashima, Y. et al., 1994, "Development of CO_2 Compressor for Fertilizer Plant", *Mitsubishi Heavy Industries Technical Review*, Vol. 31, No. 2, pp. 130-133.

[4] Yamauchi, H., Seino, H., and Yasuda, K., 2002, "Experimental and Theoretical Study of Structure-Acoustic Coupling System (Acoustic Tube with a Flexible Panel at the One End)", *Proceedings of the 12th JSME Design & Systems Conference*, No. 02-31, pp. 342-345.

[5] Yohei, M. et al., 2008, "Natural Frequencies of Centrifugal Compressor Impellers for High Density Gas Applications", *Proceedings of ASME 2008 International Mechanical Engineering Congress and Exposition*, No. IMECE2008-67278, pp. 107-114.

[6] Yuji, K. et al., 1983, "Vibration of Rotating Bladed Disc Excited by Stationary Distributed Forces", *Transactions of the Japan Society of Mechanical Engineers Series C*, Vol. 49, No. 439, pp. 307-313.

[7] *Release 10.0 Documentation for ANSYS*, ©2005 SAS IP,Inc.

[8] PROPATH Group, 2002, "W-PROPATH:Single Shot P-PROPATH on Web Page." <http://www2.mech.nagasaki-u.ac.jp/PROPATH/index.html> [2010, November 15].

[9] Kang, N. and Raman, A., 2004, "Aeroelastic Flutter Mechanisms of a Flexible Disk Rotating in an Enclosed Compressible Fluid", *Transactions of the ASME, Journal of Applied Mechanics*, Vol. 71, pp. 120-130.

